Data-model comparison of soil-water $\delta^{18}O$ at a temperate site in N. Spain with implications for interpreting speleothem $\delta^{18}O$

Laia Comas-Bru [1,*] and Frank McDermott [1,2]

[1] UCD School of Earth Sciences, University College Dublin, Belfield, Dublin 4, Ireland
[2] UCD Earth Institute, University College Dublin, Belfield, Dublin 4, Ireland.
[*] Corresponding author: laia.comasbru@ucd.ie

Available online 29th September 2015
In Press, Accepted Manuscript

Highlights:

- New monthly time-series soil-water $\delta^{18}O$ data for a temperate site
- Only 14% of monthly range in rainfall $\delta^{18}O$ preserved in 60 cm soil waters
- Soil-water $\delta^{18}O$ values at 60 cm depth show the anti-phase seasonal trends relative to rainfall
- $\delta^{18}O$ simple evapotranspiration models on a monthly basis underestimate effective summer recharge.

Abstract

An understanding of how seasonal and longer-term $\delta^{18}O$ signals in meteoric precipitation ($\delta^{18}O_p$) are modified by percolation through soils is essential to link temporal changes in speleothem $\delta^{18}O$ to surface climatic conditions. This study focuses on modifications that occur in a relatively thick soil above a temperate cave site (La Garma, N. Spain). Monthly soil-water $\delta^{18}O$ ($\delta^{18}O_{sw}$) values at a depth of 60 cm through the year is only 14% of the range in $\delta^{18}O_p$, implying substantial homogenisation and attenuation of seasonal signals. A striking feature is that $\delta^{18}O_{sw}$ values at 60 cm depth are lowest in summer and highest in winter, the opposite (anti-phase) to that observed in rainfall. Soil-water residence times of up to circa 6 months in the upper 60 cm of soil, and a matrix flow, piston-type infiltration behaviour with mixing is inferred. Evaporative effects on recovered soil-water $\delta^{18}O$ are minimal at this wet temperate site, in contrast with published results from arid and semi-arid sites. A soil-water model is presented to estimate monthly $\delta^{18}O_{sw}$ as a function of air temperature and $\delta^{18}O_p$, incorporating effects such as variations in the amount of infiltrated water, changes in the ratio between evaporation and transpiration, mixing with antecedent soil moisture and small enrichments in ^{18}O linked to evaporation and summer moisture deficits. Our model reproduces the observed $\delta^{18}O_{sw}$ results, and produces $\delta^{18}O_{sw}$ outputs in excellent agreement with $\delta^{18}O$ data for two monitored drip-water sites at La Garma cave that exhibit seasonal $\delta^{18}O$ variability. We conclude that simple evapotranspiration models that permit infiltration during months that have a positive hydrological balance only tend to under-estimate summer rainfall contributions. Overall, the study provides an improved framework for predicting $\delta^{18}O_{sw}$ trends at temperate sites such as La Garma that have a relatively thick soil cover, as well as for understanding seasonal ranges and trends in $\delta^{18}O$ in cave drip-sites.

Keywords: Soil-water $\delta^{18}O$; La Garma cave; stable oxygen isotopes; modelling.
doi: 10.1016/j.jhydrol.2015.09.053

I. Introduction

Oxygen isotope ratios in precipitation ($\delta^{18}O_p$) correlate with key climate variables such as air temperature, precipitation amount and relative humidity on a range of spatial and temporal scales (Dansgaard, 1964; Merlivat and Jouzel, 1979; Rozanski et al., 1993). Such empirical relationships underpin palaeoclimate reconstructions based on $\delta^{18}O$ variations in speleothems (McDermott, 2004; Fairchild et al., 2006), pedogenic and lake carbonates (Cerling and Quade, 1993; Leng and Marshall, 2004), and tree rings (McCarroll and Loader, 2004; Xu et al., 2011). However, correct attribution of $\delta^{18}O$ variations to specific climate variables requires a detailed proxy- and site-specific understanding, because multiple factors influence the $\delta^{18}O_p$ signal and how it is ultimately recorded. In the case of speleothems, this requires, *inter-alia*, a good understanding of the dynamic and potentially complex mixing behaviour of infiltrating meteoric water in soils and the unsaturated zone of karst systems (Williams, 2008; Baker and Bradley, 2010; Bradley et al., 2010; Baker et al., 2012; Jex et al., 2013; Moerman et al., 2014; Genty et al., 2014).

Recently, two forward models that predict cave drip-water $\delta^{18}O$ based on $\delta^{18}O_p$ inputs and climate variables such as air temperature and precipitation amount have been published (Baker and Bradley, 2010; Wackerbarth et al., 2010). Forward modelling is preferable to simpler approaches that assume stationary relationships between speleothem O isotope ratios and $\delta^{18}O_p$ but it requires assumptions regarding potential isotope fractionation and water infiltration processes within the soil zone that are based on simple quantification of potential evapotranspiration that require validation, particularly in temperate regions. Much of the previous work on the $\delta^{18}O$ of soil-water ($\delta^{18}O_{sw}$) has focused on arid and semi-arid regions where evaporation causes ^{18}O enrichment as a result of diffusion of water to the atmosphere (Zimmermann et al., 1967; Barnes and Allison, 1984; Fontes et al., 1986; Shurbaji et al., 1995; Mathieu and Bariac, 1996; Hsieh et al., 1998; Newman et al., 1997; Gazis and Feng, 2004). In some semi-arid regions, these effects have been invoked to explain some of the observed $\delta^{18}O$ variability in cave drip-waters (Ayalon et al., 1998; Cuthbert et al., 2014). By contrast, comparatively little data are available for seasonal $\delta^{18}O_{sw}$ variability in temperate regions (Robertson and Gazis, 2006; Gehrels et al., 1998). The evolution of $\delta^{18}O_{sw}$ at temperate sites is likely to differ from that at arid and semi-arid sites because a positive soil-water balance may exist for much of the year and evaporative effects are consequently less important. On the other hand, unlike arid regions where pre-existing soil-water moisture is largely absent (e.g. Hsieh et al., 1998), temperate zone soils may retain a fraction of isotopically enriched soil-water during the dry season which can affect the isotopic evolution of soil-waters during the subsequent wet season.

The infiltration regime (e.g. slow matrix flow vs. rapid macropore flow) also exerts a control on $\delta^{18}O_{sw}$ variations with depth (Tooth and Fairchild, 2003). In some cases, non-synchronous variation in $\delta^{18}O_{sw}$ and $\delta^{18}O_p$ have been demonstrated largely absent (e.g. Gehrels et al., 1998; Tang and Feng, 2001; Gazis and Feng, 2004; Li et al., 2007), associated with slow matrix flow and piston-like behaviour in which more recently recharged water pushes older water deeper into the soil profile. In other cases, the oxygen isotopic composition of shallow soil-waters closely follows that of precipitation inputs, but individual strong precipitation events with low $\delta^{18}O_p$ have an immediate impact on $\delta^{18}O_{sw}$ to depths of 60 cm indicating by-pass, macro-pore flow behaviour (Brodersen et al., 2000). A related, but poorly understood issue is the extent to which mixing of waters within the soil zone, as distinct from within the unsaturated zone of the underlying bedrock, can partly homogenise seasonal or longer time-scale variability in $\delta^{18}O_p$ in the water that percolates into caves. An understanding of the processes causing this observed attenuation of the $\delta^{18}O_{sw}$ signal is important if speleothem time-series oxygen isotope data can be sampled and analysed at a finer temporal resolution than the timescale of homogenisation, or if the climate

signal of interest has a strong seasonal expression (e.g. inter-annual variability in winter $\delta^{18}O_p$ associated with changes in the North Atlantic Oscillation; Baldini et al., 2008; Comas-Bru and McDermott, 2014). In this study, oxygen isotope ratios have been measured in rain and soil-waters that were sampled monthly above La Garma cave in N. Spain (Figure 1). To better understand the interplay between the various soil zone processes discussed above (evaporation, infiltration mechanisms and mixing), a simple soil-water model has been constructed to assess the extent to which the observed soil-water monthly variability can be estimated. Overall, this study provides improved insights into the temporal relationships between $\delta^{18}O_{sw}$ and $\delta^{18}O_p$ at different depths on seasonal timescales at a temperate site with a thick soil cover (>1m).

II. Site description and methods

I. Description of the study site

La Garma cave in N. Spain (43.43°N; 3.67°W) is located in Monte de la Garma, a low hill (186 m of altitude) of approximately three hectares situated 5 km from the mouth of the River Miera in the Cantabrian village of Omoño (Ribamontán al Monte) on the eastern side of Santander Bay (Northern Spain). The cave is part of a complex system of karstic galleries developed in Lower Cretaceous (Aptian) biomicritic limestones overlain by a laterally continuous c.150 m thick umbrisol (Jackson, 2009). The Lower Gallery at c. 80 metres above sea level, is overlain by approximately 85-90 metres of limestone at the drip-water sampling points discussed below (Figure 1). The cave has developed largely along a NE-SW trending fault (Baldini, 2007). Drip-water sites in the cave both on and away from the fault zone have been monitored in previous studies (Baldini, 2007; Jackson, 2009; Baldini et al., 2015) and data from these studies provide additional tests for the soil-water infiltration/recharge model developed here. The area above the cave in which soil-water samplers were placed is partly vegetated with trees and undergrowth. The umbric soil with a hummus-rich surface layer is typical of that found under forest cover in high rainfall regions of Western Europe (WRB, 2014). Soil thickness varies across Monte de la Garma (typically 60 to 150 cm).

II. Regional Climate

Hourly air temperature and precipitation data for Santander Airport station (43.25°N, 3.49°W; 52 m.a.s.l.), located 12.2 km from the sampling site, was provided by the Spanish Meteorological Institute (AEMET). The mean annual air temperature is 14.67°C, and the long-term annual precipitation is 1204 mm, with a monthly annual range of 3.84°C and 309.62 mm (1997-2013), respectively. According to the Köppen-Geiger climate classification scheme (Kottek et al., 2006), the site is type "Cfb". This corresponds to areas with a warm temperate climate (coldest month is -3 to 18°C), fully humid (no dry summer or dry winter), a warm summer (mean temperature of the warmest month <22°C, and a minimum mean temperature of 10°C in at least four months). Whereas mean monthly air temperatures during the sampling period closely follow the long term means, large deviations in rainfall amounts are observed for some months (Figure 2). For example, the site experienced a wetter than average winter (January and February 2013), and some exceptional storms (>30 mm/day) occurred in October 2012, November 2012, March 2013, April 2013 and May 2013.

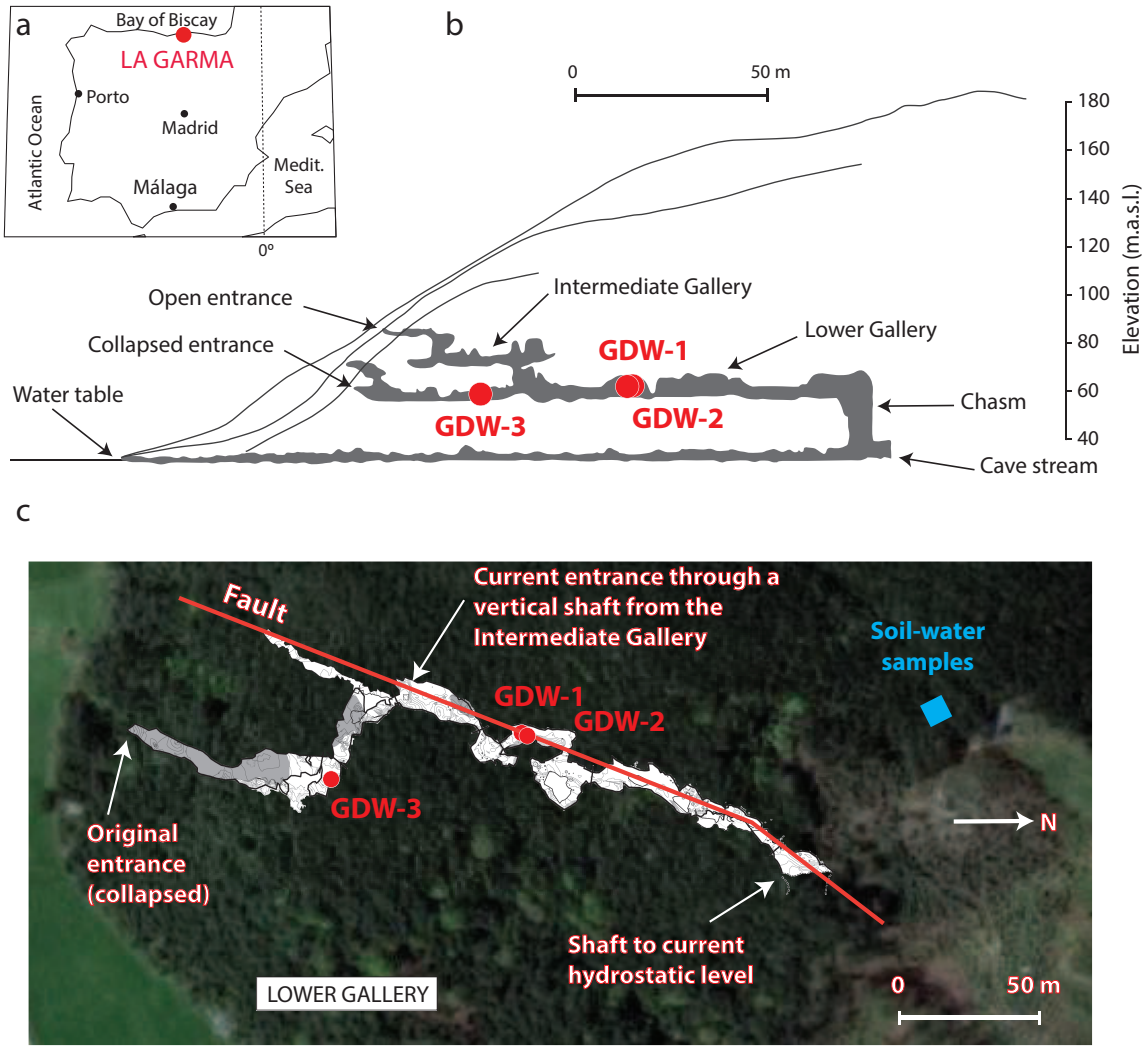

Figure 1: *(a) Location of La Garma cave (43.43°N 3.67°W) within the Iberian Peninsula. (b) Cross-section of La Garma cave showing the position of drip sites GDW-1, GDW-2 and GDW-3 relative to the cave galleries. (c) Plan view of the Lower Gallery, showing the soil-water and drip-site locations. Diagrams (b) and (c) have been modified after Arias and Ontan (2013). Aerial view in panel (c) from Google maps (2015).*

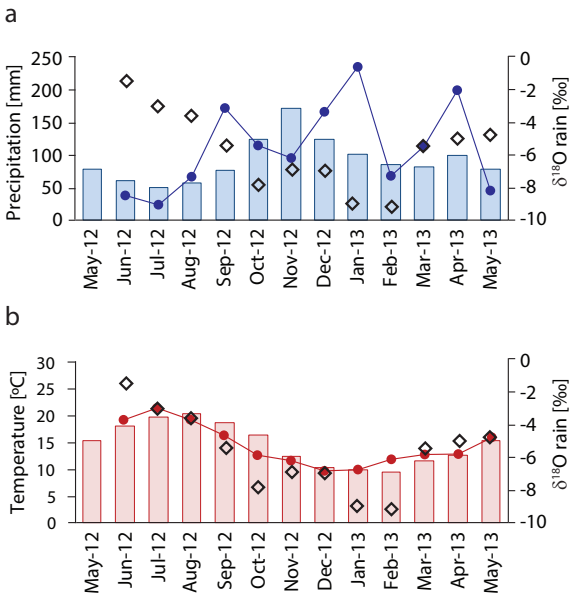

Figure 2: *Time series of precipitation, air temperature and rainfall $\delta^{18}O$ during the sampling periods (data symbols) compared with their long term means (vertical bars). (a) Precipitation amount in blue (left y-axis) and $\delta^{18}O$ as open black diamonds (right y-axis). (b) Air temperature in red (left y-axis) and $\delta^{18}O$ as open black diamonds (right y-axis). Precipitation and air temperature data were provided by the Spanish Meteorological Institute (AEMET) for the Santander Airport station.*

III. Sample collection and analysis

Rain and soil-water samples were collected at monthly intervals above La Garma cave from June 2012 to May 2013. For operational reasons, the rainfall and soil-water sampling points were located at a point on the surface that is approximately 150 metres north of the main cave galleries (Figure 1, inset). Rain water was collected in accordance with the Global Network of Isotopes in Precipitation protocols (IAEA/WMO, 2014). Soil-waters were collected using Standard 1900 ceramic-cup soil-water samplers from Soil moisture Equipment Corp. at 15 cm (S1), 30 cm (S2) and 60 cm (S3). Each soil-water sample represents the integrated moisture for the period between vacuum/collection dates. Due to operational problems and/or the occurrence of soil-moisture deficits, it was not possible to retrieve soil-water samples for all of the planned sampling intervals (Table S1). Oxygen isotopic analysis of the water samples were conducted at the Stable-Isotope Laboratory (SILLA) of the University of Birmingham using an Isoprime continuous flow Isotope-Ratio Mass Spectrometer (CF-IRMS).The samples were equilibrated at 23°C with a 5% CO_2 headspace for 7 hours before analysis by CF-IRMS (Bieroza et al., 2014). Analytical precision is estimated to be 0.04‰ for $\delta^{18}O$ and 0.48‰ for δD. The hydrogen and oxygen isotope ratios (D/H, $^{18}O/^{16}O$) are expressed as ‰ values relative to V-SMOW.

IV. Soil-water model

Not all of the precipitation that falls on a soil is available for infiltration, and so a weighting coefficient, I_m, that accounts for the fraction of infiltrating water each month was applied to model the monthly $\delta^{18}O_{sw}$. The oxygen isotopic enrichment of the soil-water by evaporation is

described by a fractional distillation process under equilibrium conditions between water vapour and soil-water using a Rayleigh equation (Rayleigh, 1896). The isotope ratio of the infiltrating soil-water is given by Hoefs (1997):

$$\delta^{18}O_{sw} = \delta^{18}O \cdot I^{(\alpha-1)\cdot f_e} \quad (1)$$

where, $\delta^{18}O$ is the isotopic composition of the initial water in the soil; $\delta^{18}O_{sw}$ is the isotopic composition when a fraction, I_m, remains; the fractionation factor α is given by Majoube (1971); f_e is the ratio between water lost by evaporation and transpiration.

The monthly weighting coefficient, I_m, was estimated using information about the monthly soil moisture budget as described below. The monthly potential loss of water due to direct evaporation and transpiration (PET) for the area above the site was estimated using a water-balance model (Thornthwaite, 1948) as implemented in the USGS Thornthwaite model (McCabe and Markstrom, 2007). This model uses the Hamon equation (Hamon, 1961) to estimate PET, and it assumes that none of the soil or plant surfaces is water-limited and that the extent to which PET occurs depends mainly on air temperature (Thornthwaite, 1948; Mather, 1978):

$$PET_m = 13.97 \cdot d \cdot D^2 \cdot W_t \quad (2)$$

where PET_m is monthly potential evapotranspiration in mm, d is the number of days in a month, D is the mean monthly hours of daylight in units of 12 hours, and, W_t is a saturated water vapour density term, in grams per cubic meter, calculated by:

$$W_t = (4.95 \cdot e^{(0.062 \cdot T)}) / 100 \quad (3)$$

where T is the mean monthly temperature in degrees Celsius (Hamon, 1961). Since water loss does not always proceed at the potential rate (PET_m) because of water supply limitations, the actual evapotranspiration (AET_m) is estimated from PET_m, monthly precipitation amount (P_m), soil moisture storage (ST_m) and soil moisture storage withdrawal (STW_m) using the Thornthwaite model (McCabe and Markstrom, 2007). In this methodology, the amount of moisture that can be removed from the soil (STW_m) depends on the moisture remaining in the soil from the previous month ($ST_{(m-1)}$), the soil moisture capacity (STC) and the difference between P_m and PET_m (Thornthwaite model; McCabe and Markstrom, 2007):

$$STW_m = ST_{(m-1)} - [abs(P_m - PET_m) \cdot (ST_{(m-1)} / STC)] \quad (4)$$

The Thornthwaite method is known to overestimate PET in humid areas (Schiff, 1975; Chen et al., 2005; Trajkovic and Kolakovic, 2009). The alternative Penman-Monteith methodology recommended by the Food and Agriculture Organization of the United Nations (Allen et al., 1998) yields PET values closer to measured values, but in the absence of relative humidity and wind speed data required for the Penman-Monteith methodology, the Thornthwaite method was used.

Calculations were done on a monthly basis, beginning with the soil moisture budget for January, assuming that the previous December had no soil moisture deficit. For those months in which water is supplied by frequent precipitation events, AET is assumed to equal PET. On the other hand, AET differs from PET when the soil moisture deficit falls below a critical threshold where vegetation has difficulty transpiring.

If the amount of infiltrated water (ST_m=P_m-AET_m), plus the soil moisture remaining from the previous month exceeds the STC, this surplus water is considered to be available for infiltration, and only the STC component is carried over in the computations for the following month. On the other hand, if the amount of infiltrated water (ST_m=P_m-AET_m), plus the soil moisture available

from the previous month is less than the STC, no infiltration occurs, and the remaining moisture is allowed to mix with the infiltrated water of the following month. If a moisture deficit persists for several months, moisture stored initially in the STC decreases gradually until for example a precipitation event in autumn replenishes it, and eventually, a water surplus is re-established to allow infiltration to begin again. Otherwise, the monthly weighting coefficient could reach zero if a prolonged drought lasted for several months.

Consequently, if $ST_m+ST_{(m-1)}>STC$, infiltration occurs and

$$I_m = (ST_m + STC) / (P_m + STC) \quad (5)$$

where STC is the contribution of the antecedent moisture (i.e. the moisture that did not infiltrate and is carried over from the previous month). On the other hand, no infiltration occurs if $ST_m+ST_{(m-1)}<STC$, and in that case

$$I_m = (ST_m + ST_{(m-1)}) / (P_m + ST_{(m-1)}) \quad (6)$$

In the soil-water model, moisture of different isotopic compositions (i.e. one month, ST_m, and the preceding month, $ST_{(m-1)}$) is thus mixed in different proportions, depending on the balance between antecedent soil moisture and recharged water for each month. Isotopic mixing is conservative and a simple mass-balance model is used to calculate the $\delta^{18}O$ of the infiltrated water. To account for different degrees of $\delta^{18}O_{sw}$ homogenisation at depth, the model $\delta^{18}O_{sw}$ output described above is allowed to mix with antecedent water for several months at each depth (15, 30 and 60 cm). Mixing periods of 2 to 5 months have been tested (Supplementary Figure S1). The monthly weighting factors used to compute the mixing are based on the relative contributions of each month to the total moisture according to the soil-water budget described above (Table 1).

	%	JAN	FEB	MAR	APR	MAY	JUN	JUL	AUG	SEP	OCT	NOV	DEC
SW-A (60 cm)	JAN	28.7									3.3	35.6	32.3
	FEB	47.7	20.5									7.5	23.8
	MAR	53	37.5	0.1									12.5
	APR	10.3	35.5	16.8	37.3								
	MAY		8.3	13.8	47.8	30.1							
	JUN												
	JUL												
	AUG												
	SEP												
	OCT										100		
	NOV										44.9	55.1	
	DEC									0	22.2	68.1	9.7
SW-B (60 cm)	JAN	8.7							1.15	6.2	33.1	33.6	18.1
	FEB	23.1	9.2							1.5	14.3	27.6	26.1
	MAR	32.7	17.6	1.4							4.7	17.9	26.1
	APR	33.4	31.2	7.3	4.3							6.5	16.6
	MAY	17.7	31	17.9	19.5	9.4							4.2
	JUN	8	24	21.1	29	16.9	0.6						
	JUL		12.3	19.5	36.2	29.5	2.1	0.3					
	AUG			9.5	37.2	42.9	5.6	3.7	1				
	SEP				10.7	30	22.5	15.8	11	10.8			
	OCT					4.3	8.1	11.1	12.6	24.2	39.8		
	NOV						2.5	4.9	8.3	20.5	49	16.3	
	DEC							1.7	4.2	14.8	48.1	25.8	5.9

Table 1: *Monthly contributions of $\delta^{18}O_p$ to modelled monthly $\delta^{18}O_{sw}$ with SW-A and SW-B models, in percentages.*

Although soil macropore or preferential bypass flows have been reported in some studies at depths of up to 50 cm, following intense rainfall events (Tang and Feng, 2001; Gazis and Feng, 2004), our monthly resolved soil-water $\delta^{18}O$ data does not require them to successfully estimate

the observed $\delta^{18}O$ data. Bypass infiltration processes within the unsaturated zone are also featured in full karst hydrogeological models designed to account for cave drip-water $\delta^{18}O$ variability (e.g. Baker and Bradley, 2010). However, here we emphasise here that our model is intended only to explore soil-water $\delta^{18}O$ variability in temperate zone soils at depths of up to 60 cm, and therefore, does not include processes in the unsaturated zone of the bedrock. Comparison of modelled and observed $\delta^{18}O_{sw}$ data at 60 cm with seasonal drip-water $\delta^{18}O$ variability (see section 4) is made on the basis that the monitored drip-sites GDW-1 and GDW-2 are located along a fault zone that provides a conduit for rapid transit through the bedrock (Figure 1; Baldini et al., 2015). In effect, our model describes a simple piston-flow system, dominated by matrix flow in which new precipitation pushes existing soil moisture deeper into the soil profile, with variable degrees of mixing with pre-existing soil moisture, a fraction of which may be enriched in ^{18}O as a consequence of evaporation.

A sensitivity test using different values of f_e was employed to assess the model sensitivity to this parameter. For reference, the study by Wackerbarth et al. (2010) in central Germany with the same climate classification as the La Garma site ("Cfb" Kottek et al., 2006) used f_e=0.2 for summer (April-September) and f_e=0.5 for winter (October-March). A sensitivity analysis of various f_e values (Table 2) demonstrates that the modelled $\delta^{18}O_{sw}$ output varies only within analytical uncertainty. Thus, the f_e values from Wackerbarth et al. (2010) were used in the model. In the absence of soil-moisture capacity (STC) measurement, a value of 150 mm was used for the site. Sensitivity tests confirmed that while the model output is sensitive to the STC value it is not unduly influenced by this parameter. For example the model produced a shift to higher $\delta^{18}O_{sw}$ of 0.14‰ in the mixed 60 cm water when a STC value of 200 mm was used instead of 150 mm.

fe(Oct-Mar)	fe(Apr-Sep)	SW-A	SW-B	Comments
0.4	0.1	-6.85	-6.09	Increased seasonality
0.5	0.3	-6.84	-6.09	Values used in this study (*)
0.9	0.6	-6.83	-6.09	Decreased seasonality
0.9	0.3	-6.83	-6.09	"
0.2	0.5	-6.84	-6.09	Inverted seasonality
0.1	0.1	-6.84	-6.09	No seasonality
0.3	0.3	-6.84	-6.09	"
0.5	0.5	-6.84	-6.09	"
1	1	-6.83	-6.09	"

Table 2: *Output of the SW-A and SW-B models at 15 cm using different values of the fraction of water lost through evaporation with respect to the total water loss (f_e). (*) Same values as in Wackerbarth et al. (2010).*

III. Results

I. Rain and soil-water $\delta^{18}O$

Monthly rainfall $\delta^{18}O$ values at the La Garma site range from -9.15 to -1.49‰ (VSMOW), with highest values occurring during the summer months (Figure 3). The mean annual weighted $\delta^{18}O_p$ of the rainfall samples is -6.39‰. Significant correlations are observed between $\delta^{18}O_p$ and both mean air temperature (ρ=0.80; significant at 99%) and rainfall amount (ρ=-0.60; significant at 95%). These correlations are consistent with longer $\delta^{18}O_p$ series and meteorological data from the Santander Airport GNIP station (IAEA/WMO, 2014), which yield ρ values of 0.56 and -0.56

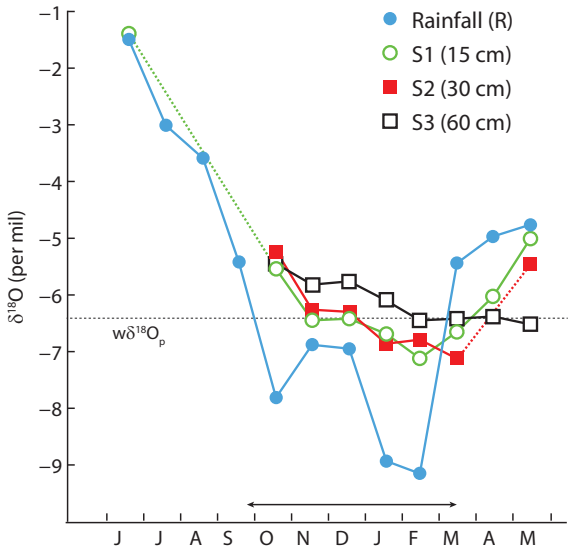

Figure 3: *Time series of the $\delta^{18}O_p$ and $\delta^{18}O_{sw}$ samples. Double arrowed horizontal line indicates winter months for easier visualisation. Dashed horizontal line is the mean annual weighted $\delta^{18}O_p$ (-6.39‰)*

(significant at 99%) for air temperature and rainfall amount, respectively, for the period February 2000 to November 2010. The rainfall samples are offset slightly to lower δ^{18}O compared with most of the GNIP (n=130) rainfall samples on which the Local Meteoric Water Line (LMWL) is based (Figure 6a). A similar offset with respect to the LMWL is observed in the soil-water samples (Figure 6b). None of the soil-water data plot below the LMWL.

Over the study period, the $\delta^{18}O_{sw}$ at 15 cm and 30 cm data follow the rainfall δ^{18}O trends although they are lagged by one to two months, and exhibit a much reduced range (5.7‰ at 15 cm, and 1.9‰ at 30 cm depth; Figure 3). $\delta^{18}O_{sw}$ data for the deeper (60 cm) samples are even more strongly lagged (∼3 months) and the range is more strongly attenuated (1.08‰) compared with that of the rainfall (7.66‰). At this soil depth, the range in $\delta^{18}O_{sw}$ is only about 14% of that of $\delta^{18}O_p$ (Figures 3 and 4a).

Depth profiles (Figure 4a), show a tendency for higher $\delta^{18}O_{sw}$ values in the shallow samples (15 cm) compared with the deeper samples (30 and 60 cm) during the summer. The opposite is observed during winter, when the lowest $\delta^{18}O_{sw}$ values occur at shallow levels, and the highest values are found at depth in the soil profile. An important result in the context of water that is potentially available for aquifer recharge is that for most months of the year, $\delta^{18}O_{sw}$ values at 60 cm depth were appreciably higher than the mean annual weighted δ^{18}O of the rainfall (-6.39‰, dashed lines in Figure 3 and 4a), with highest values retrieved during some of the winter months (November to January), a time when $\delta^{18}O_p$ is characterised by low values). Because we do not have information about temporal variations in the soil moisture content at 60 cm depth, it is not possible to calculate the weighted mean annual δ^{18}O value for the soil-waters. On the basis of a Thornthwaite water balance model (McCabe and Markstrom, 2007, Figure 4b) (McCabe and Markstrom, 2007, Figure 4b), soil moisture deficits occur between May and August. No soil-water samples could be retrieved for August and September at any depth (Supplementary Table 1) despite the occurrence of some rainfall events >10 mm/day during this period (Figure 2a).

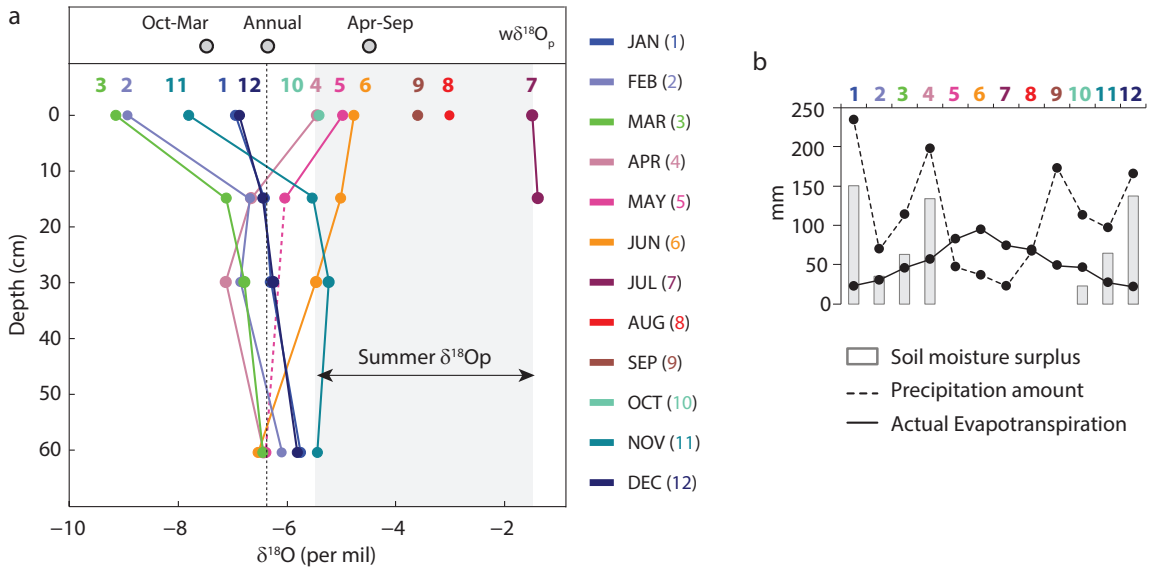

Figure 4: *Depth profiles of measured $\delta^{18}O_{sw}$ and water balance plots. (a) $\delta^{18}O_p$ (at 0 cm depth) and $\delta^{18}O_{sw}$ depth profiles (S1: 15cm, S2: 30cm and S3: 60 cm). Weighted mean winter, annual and summer $\delta^{18}O_p$, calculated with the rainfall data presented in this study, are indicated at the top of the panel. Grey area in (a) indicates the range of summer (April-September) $\delta^{18}O_p$. (b) Water balance plot calculated with the mean air temperature and precipitation amount for the sampling intervals using a Thornthwaite Monthly Water Balance Model (McCabe and Markstrom, 2007).*

II. Soil-water model results

Modelled monthly $\delta^{18}O_{sw}$ values for the shallow horizon (15 cm) fall within the observed range except for some months (Figure 5a). For instance, the slightly higher $\delta^{18}O$ value of the July S1 sample compared with its rainfall counterpart (Supplementary Table S1 and Figure 4a) is not reproduced in our model, and the modelled output at S1 is lower than the observations (Figure 5a,b). In contrast, excellent agreement is observed between the model output and observations at greater depths (30 and 60 cm; Figure 5a,c,d), where only the output of the model at 30 cm is marginally lower than observed (Figure 5c).

Consistent with the observations, modelled $\delta^{18}O_{sw}$ values at depths (30 and 60 cm) for the winter months are higher than the observed mean annual weighted $\delta^{18}O$ of the rainfall, while the opposite occurs in the model output from summer months (Figure 5a). Mixing periods of 2, 3 and 3 months are required at 15, 30 and 60 cm respectively, to reproduce the observed monthly $\delta^{18}O_{sw}$ patterns. This indicates that homogenisation of the monthly $\delta^{18}O_p$ signal at 60 cm depth occurs over about 6 months (Figure 5b-d and Supplementary Figure S4). Table 1 illustrates the monthly contribution of $\delta^{18}O_p$ to $\delta^{18}O_{sw}$ at 60 cm. Owing to the mixing factors implied by the soil-water model, the October - March (April -September) contribution to the annual $\delta^{18}O_{sw}$ at 60 cm is 61.4% (38.6%). Approximately 21% of the October - March $\delta^{18}O_{sw}$ signal at 60 cm reflects residual inputs from summer rainfall.

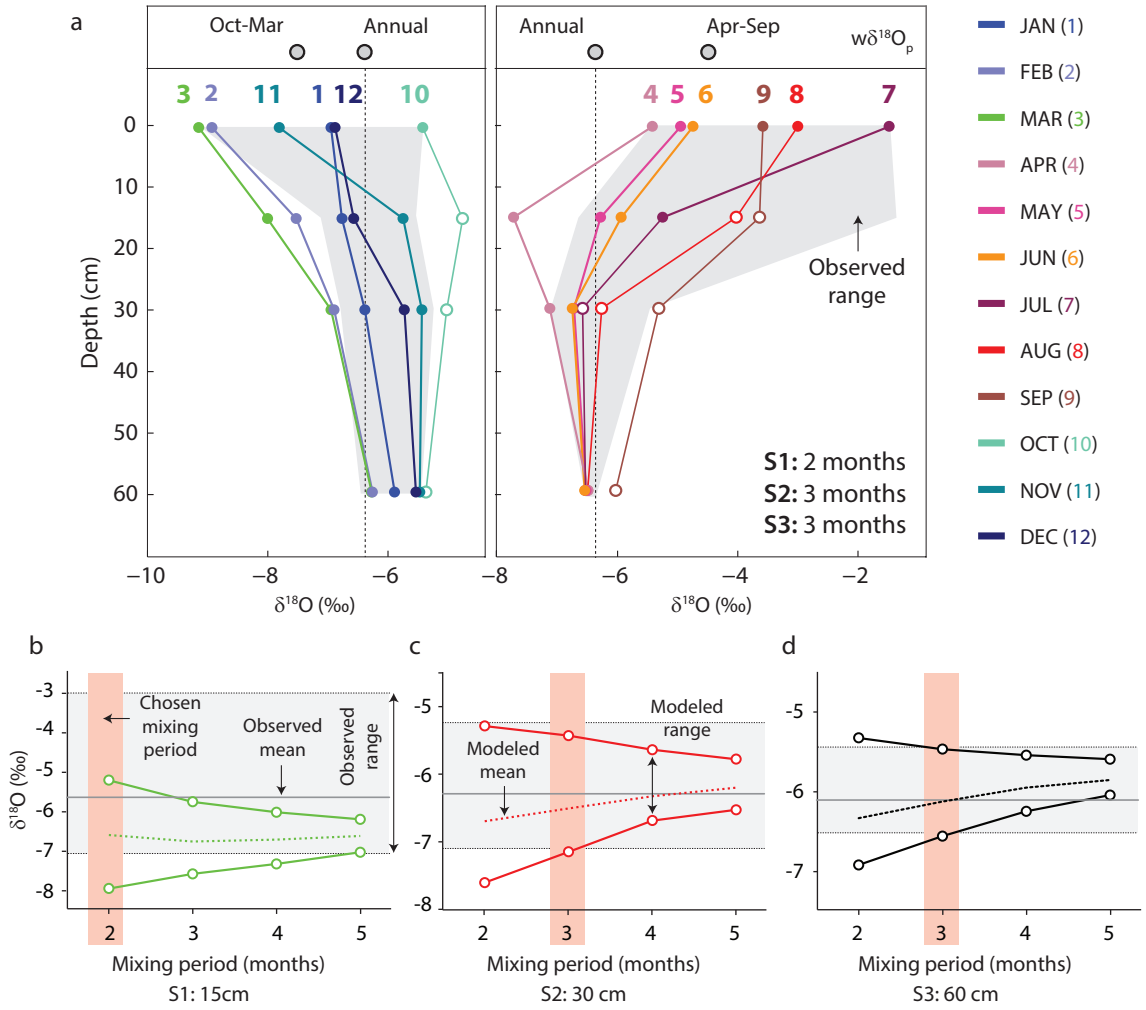

Figure 5: *Results of the soil-water model using STC=150 mm, f^e=0.2 for summer (April-September) and f^e=0.5 during winter (October-March). (a) Depth profiles of modelled monthly $\delta^{18}O_{sw}$. Grey shaded area in (a) is the range of measured monthly $\delta^{18}O_p$ and $\delta^{18}O_{sw}$ (as in Figure 4). Open symbols in (a) represent depths/months when samples could not be retrieved and thus, are not included in the grey shaded area. Mean winter, annual and summer $\delta^{18}O_p$, calculated with the rainfall data presented in this study, are indicated at the top of the panel. (b) Modelled $\delta^{18}O_{sw}$ range and mean at 15 cm (S1) compared to observations for a number of mixing months (x-axis); (c) same as (b) for 30 cm depth (S2); (d) same as (b and c) for 60 cm depth (S3). The applied mixing periods (x-axis in a, b and c) are calculated as illustrated in Supplementary Figure S1. For example, the mixing applied in S2 (c) uses as input the results obtained with the mixing period chosen for S1 (b). The same is true for S3 (d) and the results from S2 (c). $\delta^{18}O_{sw}$ ranges and means in (b), (c) and (d) are calculated for the same number of months as available observed data (i.e. open symbols in (a) are omitted in the calculations).*

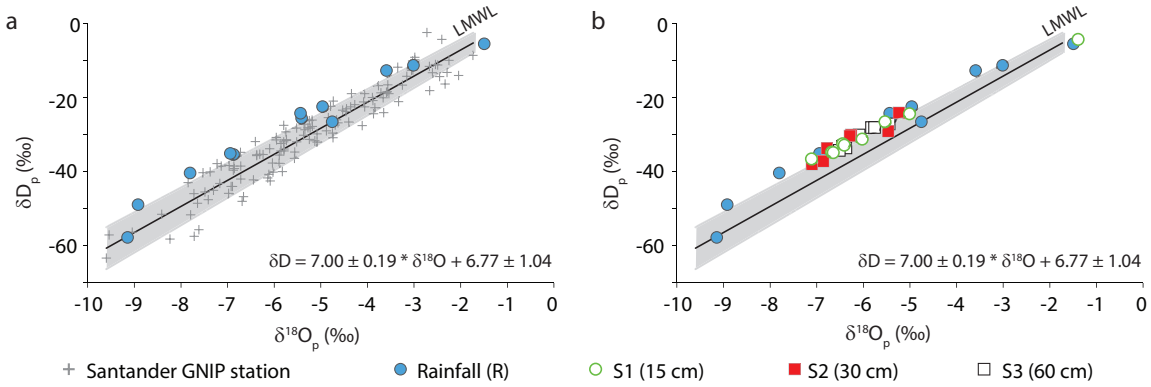

Figure 6: *Isotopic compositions of rainfall and soil-water samples. (a) Rainfall samples collected in this study and all the monthly samples available from the GNIP station at Santander Airport (43.48°N 3.80°W; IAEA/WMO, 2014, grey crosses). The LMWL was derived using the 130 unweighted samples from the GNIP station; (b) Rain and soil-water samples collected in this study compared to the LMWL. The shaded areas show the 95% confidence intervals of the LMWL and its equation is shown in each panel.*

IV. Discussion

Our results differ from the majority of studies that were completed at arid and low rainfall sites (Barnes and Allison, 1984; Fontes et al., 1986; Shurbaji et al., 1995; Mathieu and Bariac, 1996; Hsieh et al., 1998; Newman et al., 1997; Gazis and Feng, 2004), because unlike the temperate zone site studied here, these are characterised by little or no antecedent moisture at the end of the dry season. The steep slope defined by our soil-water data on a D/H vs. $\delta^{18}O$ diagram (Figure 6) and the absence of significant departures from the Local Meteoric Water Line (LMWL; Figure 6) provides little evidence for evaporative isotopic enrichment of soil-waters prior to recharge at this temperate site, in contrast with results from drier sites (Hsieh et al., 1998; Robertson and Gazis, 2006). This validates results from Bradley et al. (2010), where evaporation is found to be negligible at relatively temperate and wet sites. However, the presence of vegetation could in principle induce additional isotopic enrichment in soil-waters if partly evaporated throughfall water is an important component (Brodersen et al., 2000). We cannot rule out the possibility that the absence of recoverable water in a few of the summer months may have resulted from evapotranspiration or as a result of insufficient vacuum in the samplers to extract soil water.

Two important results arise from our study. First, to account for the observed $\delta^{18}O_{sw}$ data, some infiltration of summer rains into the deeper (circa 60 cm) soil profile must occur, despite indications from simple "Thornthwaite-type" evapotranspiration models that soil moisture deficits occur in summer (Figure 4b). This result is consistent with recent observations of cave drip-water $\delta^{18}O$ at two temperate-zone cave sites in SE and SW France (Genty et al., 2014) and it highlights the limitations of simple "Thornthwaite-type" models for forward modelling of soil-water moisture $\delta^{18}O$ at temperate sites. The study by Genty et al. (2014) demonstrated that modelled drip-water values would be much lower than the weighted mean $\delta^{18}O_p$ value if only those months with a modelled positive water balance had contributed to the cave drips. A similar requirement for contributions to deep soil-waters by summer precipitation, despite a modelled moisture deficit, was observed in the study of Gehrels et al. (1998) in temperate central Netherlands. Overall, this appears to be a robust observation at temperate zone sites. In part this discrepancy may arise because, as introduced earlier, "Thornthwaite-type" models overestimate potential evapotranspiration in relatively humid climates. For example, in accordance with the

"Thornthwaite-type" estimations of soil moisture deficits (Figure 4b), no soil-waters could be retrieved for August and September at any depth (Supplementary table S1). However, the $\delta^{18}O$ depth profile for November can only be explained (and modelled) if some water from late-summer rains had remained in the soil (Figure 4a and 5a). A combination of effects could explain this observation. First, the effect of evapotranspiration on effective recharge may be overestimated as a result of using monthly data to calculate these "Thornthwaite-type" models. In this case, intense or long-duration rainfall events that could be capable of generating recharge do not appear to be effective when averaged over a month. Second, during September and October the soil was likely to have been too dry to efficiently transmit water into the sampler, despite some rain events taking place. Under these conditions water would be held too tightly by surface tension with the soil to be extracted by the samplers.

Use of a water infiltration model in which only hydrologically effective precipitation is considered (no infiltration in months with $AET_m > P_m$; e.g. as implemented in the model of Wackerbarth et al. (2010)) produced modelled annual mean $\delta^{18}O_{sw}$ values lower than the observed ranges, particularly in winter (Supplementary Figure S2a-c). It appears that simple "Thornthwaite-type" schemes that permit rainfall inputs during months with a positive hydrological balance only, produce winter-biased results because no contributions from pre-existing soil moisture is considered when the first autumn rains occur following the summer soil moisture deficit. By contrast, our model permits the summer months to have an influence on the isotopic composition of the infiltrated water because of soil water storage (STC), and it thus produces higher mean $\delta^{18}O_{sw}$ values, in better agreement with observed soil-water values (Figure 5a-c).

A second robust result is that both the measured and the model $\delta^{18}O$ values exhibit strong homogenisation of the $\delta^{18}O_p$ signal at depths of 60 cm (Figures 4 and 5). As a result, the range in $\delta^{18}O_{sw}$ at 60 cm depth is only 14% that of $\delta^{18}O_p$. Whilst this study does not aim to provide a hydrogeological karst model to estimate cave-drip water $\delta^{18}O$ values, we note that a comparable degree of attenuation has been observed in $\delta^{18}O$ values from monitored cave seepage waters at two drip-sites within La Garma cave between September 2004 and October 2005 (GDW-1 and GDW-2; Baldini et al., 2015). In these drip-sites, located along a fault zone that facilitates rapid flow (Baldini et al., 2015), the monthly drip-water $\delta^{18}O$ range is only 16% that of $\delta^{18}O_p$. Demonstration that a large degree of oxygen isotopic homogenisation can occur within the upper 1 metre of the soil zone has implications for how the soil compartments of hydrogeological forward models are designed to generate synthetic drip-water $\delta^{18}O$ time-series (e.g. Baker and Bradley, 2010). In this regard, we note that the strong attenuation of seasonal $\delta^{18}O_p$ signals observed here is relevant for karst sites that are overlain by relatively thick soils or glacial tills, but is unlikely to be relevant for karst that is overlain by thin, poorly developed soils.

Despite the observed large degree of attenuation of the original $\delta^{18}O_p$ signal at a depth of 60 cm, it is clear that seasonal changes of $\delta^{18}O_{sw}$ are ultimately driven by the seasonal $\delta^{18}O_p$ variability. During the sampling period, summer $\delta^{18}O_p$ values were higher than winter values by 2.97‰, but our soil-water data show the opposite trend at deeper soil horizons, with $\delta^{18}O_{sw}$ values being lower during summer in comparison to winter months (by 0.52‰; Figure 4a). This anti-phase behaviour and substantial attenuation of the $\delta^{18}O_{sw}$ signal relative to $\delta^{18}O_p$ indicates an average soil-water infiltration time of about 6 months, consistent with the mixing factors required by our model (Supplementary Figure S1), and suggests a predominantly matrix flow, piston-type behaviour in the soil zone at this site. Similar observations were reported in drip-water $\delta^{18}O$ data from La Garma cave, where the mean winter (DJF) $\delta^{18}O$ values were unexpectedly higher than the summer (JJA) means by 0.50 and 0.32‰ at the GDW-1 and GDW-2 drip-sites, respectively (Baldini et al., 2015). Baldini et al. (2015) estimated the drip-water residence time to be of 7.5 months for the GDW-1 site, suggesting that the water may experience a transit time of

<2 months between the deepest soil horizon described in our model/observations (60 cm) and the monitored drip-sites GDW-1 and GDW-2. This is consistent with the previous classification of these drip-sites as "seasonal drips" (Smart and Friedrich, 1986) on the basis of their rate of discharge and coefficient of variation (Jackson, 2009). In this type of drip-site, drip-rate and discharge is determined to a larger extent by variations in annual rainfall and evaporation than by an aquifer reservoir, explaining their fast, "flashy" nature (Jackson, 2009). Palaeoclimate studies using $\delta^{18}O$ in spelothems require an understanding on how different factors affect the relationship between $\delta^{18}O$ values of contemporaneous rainwater and drip-water. In particular, our results show that by only considering how the $\delta^{18}O$ of infiltrated water is modified in the upper 60 cm of the soil, we are able to better constrain the causes of drip-water, and thus speleothem, $\delta^{18}O$ seasonal variability at least for the GDW-1 and GDW-2 drip-sites located along the fault zone at La Garma cave. It is important to note, however, that at other locations in the cave, greater attenuation of the seasonal $\delta^{18}O_p$ signals and mixing occurring over multiple years within the unsaturated zone of the karst is likely, at least at slow drip-sites such as GDW-3, located off the fault zone (Figure 1). This site exhibits a "dual porosity" aquifer system with elements of rapid response (e.g. fracture filling rise to increased hydraulic level) and a base-flow corresponding to a longer-term storage component in the aquifer as evidenced by drip-rate measurements (Supplementary Figure S3). In contrast with the GDW-1 and GDW-2 drip-sites, this slow-dripping seepage flow site displays almost constant $\delta^{18}O$ values with little or no preservation of the seasonal $\delta^{18}O_p$ signal (Baldini, 2007).

V. Conclusions

A new monthly resolved time-series dataset of soil-water $\delta^{18}O$ for three depths (15, 30 and 60 cm), coupled with contemporaneous $\delta^{18}O$ measurements on rainfall, provides new insights into the processes of rainwater infiltration and mixing in a thick umbrisol developed on karstified Cretaceous limestone in a partly forested temperate region in N. Spain. The study provides two results that are important for studies that require better constraints on the seasonal effects on infiltration of rainfall as well as the timescales of mixing in the upper 0.6 metres of a thick temperate zone soil. First, the observed temporal variations in soil-water $\delta^{18}O$ require that some stored summer rainfall must be included in the soil-water budget, even for months in which a moisture deficit is predicted by simple evapotranspiration models. The latter is consistent with results from a recent study of temporal variability in cave drip-water $\delta^{18}O$ at two French cave sites (Genty et al., 2014). A simple soil-water model driven by piston-flow, but permitting mixing between newly infiltrated and antecedent moisture closely reproduces the observed $\delta^{18}O_{sw}$ at depth in the soil. The model is quite insensitive to the balance between evaporation and transpiration, indicating that evaporation is negligible at this temperate zone site, in accordance with our D/H vs. $\delta^{18}O$ results, and with inferences by Bradley et al. (2010).

Second, seasonal scale $\delta^{18}O_p$ variability is largely homogenised and attenuated in soil-water samples collected at 60 cm depth, a feature that is also captured by our soil-water model. The muted seasonal range in $\delta^{18}O_{sw}$ (14% that of $\delta^{18}O_p$) above La Garma cave is similar to that observed a two monitored drip-sites that are located along a fault zone that provides a conduit for rapid flow (Baldini et al., 2015). As a result of a c. 6 month mixing time, $\delta^{18}O_{sw}$ values at 60 cm depth show the opposite seasonal trends compared with $\delta^{18}O_p$. Overall, this work presents an improved framework for predicting soil-water $\delta^{18}O$ trends in temperate sites that have a relatively thick soil cover, as well as for understanding seasonal trends observed in $\delta^{18}O$ of soil waters that are available to feed drip-sites within La Garma cave.

. Acknowledgements

This work was funded by Science Foundation Ireland through its " Research Frontiers Programme " (10/RFP/GEO2747). We would like to thank Patrícia Fernández Sánchez and Prof. Pablo Arias Cabal (University of Santander, Spain) for carefully collecting the samples presented here. The helpful technical advice from Mr Michael Murphy (UCD School of Earth Sciences) is greatly appreciated. The authors are grateful to the journal editor, Prof. Peter K. Kitandis and two anonymous reviews for their insightful reviews and advice that greatly improved the manuscript.

References

Allen, R. G., L. S. Pereira, D. Raes, and M. Smith (1998). *Crop evapotranspiration Guidelines for computing crop water requirements.* FAO Irrigation and Drainage. Paper 56. Rome: FAO - Food and Agriculture Organization of the United Nations.

Arias, P. and R. Ontan (2013). *Pleistocene foragers on the Iberian Peninsula: Their culture and environment.*, pp. 261–281. Mettmann: Neanderthal Museum.

Ayalon, A., M. Bar-Matthews, and E. Sass (1998). Rainfall-recharge relationships within a karstic terrain in the eastern mediterranean semi-arid region, israel: delta o-18 and delta d characteristics. *Journal of Hydrology 207*(1-2), 18–31.

Baker, A. and C. Bradley (2010). Modern stalagmite delta o-18: Instrumental calibration and forward modelling. *Global and Planetary Change 71*(3-4), 201–206.

Baker, A., C. Bradley, S. J. Phipps, M. Fischer, I. J. Fairchild, L. Fuller, C. Sptl, and C. Azcurra (2012). Millennial-length forward models and pseudoproxies of stalagmite δ^{18}O: an example from NW Scotland. *Climate of the Past 8*(4), 1153–1167. doi: 10.5194/cp-8-1153-2012.

Baldini, L. M. (2007). *An investigation of the controls on the stable isotope signature of meteoric precipitaton, cave seepage water, and holocene stalagmites in Europe*. Phd thesis, UCD School of Geological Sciences. University College Dublin.

Baldini, L. M., F. McDermott, J. U. L. Baldini, P. Arias, M. Cueto, I. J. Fairchild, D. L. Hoffmann, D. P. Mattey, W. Mueller, D. C. Nita, R. Ontanon, C. Garcia-Monco, and D. A. Richards (2015). Regional temperature, atmospheric circulation, and sea-ice variability within the younger dryas event constrained using a speleothem from northern iberia. *Earth and Planetary Science Letters 419*, 101–110.

Baldini, L. M., F. McDermott, A. Foley, and J. U. L. Baldini (2008). Spatial variability in the european winter precipitation d18o-nao relationship: Implications for reconstructing nao-mode climate variability in the holocene. *Geophysical Research Letters 35*(L04709), L04709.

Barnes, C. J. and G. B. Allison (1984). The distribution of deuterium and ^{18}O in dry soils: 3. Theory for non-isothermal water movement. *Journal of Hydrology 74*(1-2), 119–135. doi: 10.1016/0022-1694(84)90144-6.

Bieroza, M., A. Baker, J. Bridgeman, and I. Boomer (2014). Stable isotopic composition of raw and treated water. *Proceedings of the ICE - Water Management 167*, 414–429. doi: 10.1680/wama.13.00065.

Bradley, C., A. Baker, C. N. Jex, and M. J. Leng (2010). Hydrological uncertainties in the modelling of cave drip-water δ^{18}O and the implications for stalagmite palaeoclimate reconstructions. *Quaternary Science Reviews 29*(17-18), 2201–2214. doi: 10.1016/j.quascirev.2010.05.017.

Brodersen, C., S. Pohl, M. Lindenlaub, C. Leibundgut, and K. von Wilpert (2000). Influence of vegetation structure on isotope content of throughfall and soil water. *Hydrological Processes 14*(8), 1439–1448.

Cerling, T. E. and J. Quade (1993). *Stable Carbon and Oxygen Isotopes in Soil Carbonates*, pp. 217–231. American Geophysical Union. doi: 10.1029/GM078p0217.

Chen, D., G. Gao, C. Xu, J. Guo, and G. Ren (2005). Comparison of the Thornthwaite method and pan data with the standard Penman-Monteith estimates of reference evapotranspiration in China. *Climate Research 28*(2), 123–132. doi: 10.3354/cr028123.

Comas-Bru, L. and F. McDermott (2014). Impacts of the ea and sca patterns on the european twentieth century naowinter climate relationship. *Quarterly Journal of the Royal Meteorological Society 140*(679), 354–363.

Cuthbert, M. O., A. Baker, C. N. Jex, P. W. Graham, P. C. Treble, M. S. Andersen, and R. I. Acworth (2014). Drip water isotopes in semi-arid karst: Implications for speleothem paleoclimatology. *Earth and Planetary Science Letters 395*, 194–204. doi: 10.1016/j.epsl.2014.03.034.

Dansgaard, W. (1964). Stable isotopes in precipitation. *Tellus XVI 4*, 436–468. doi: 10.1111/j.2153-3490.1964.tb00181.x.

Fairchild, I. J., C. L. Smith, A. Baker, L. Fuller, C. Sptl, D. Mattey, F. McDermott, and E.I.M.F (2006). Modification and preservation of environmental signals in speleothems. *Earth Science Reviews 75*(1-4), 105–153. doi: 10.1016/j.earscirev.2005.08.003.

Fontes, J. C., M. Yousfi, and G. B. Allison (1986). Estimation of long-term, diffuse groundwater discharge in the northern sahara using stable isotope profiles in soil-water. *Journal of Hydrology 86*(3-4), 315–327.

Gazis, C. and X. Feng (2004). A stable isotope study of soil water: evidence for mixing and preferential flow paths. *Geoderma 119*(1-2), 97–111. doi: 10.1016/S0016-7061(03)00243-X.

Gehrels, J. C., J. E. M. Peeters, J. J. De Vries, and M. Dekkers (1998). The mechanism of soil water movement as inferred from o-18 stable isotope studies. *Hydrological Sciences Journal-Journal Des Sciences Hydrologiques 43*(4), 579–594.

Genty, D., I. Labuhn, G. Hoffmann, P. A. Danis, O. Mestre, F. Bourges, K. Wainer, M. Massault, S. Van Exter, E. Regnier, P. Orengo, S. Falourd, and B. Minster (2014). Rainfall and cave water isotopic relationships in two south-france sites. *Geochimica Et Cosmochimica Acta 131*, 323–343.

Hamon, W. R. (1961). Estimating potential evapotranspiration. *Journal of Hydraulic Engineering 87*, 107–120.

Hoefs, J. (1997). *Stable Isotope Geochemistry* (4th ed.). Berlin: SpringerVerlag.

Hsieh, J. C. C., O. A. Chadwick, E. F. Kelly, and S. M. Savin (1998). Oxygen isotopic composition of soil water: Quantifying evaporation and transpiration. *Geoderma 82*(1-3), 269–293. doi: 10.1016/S0016-7061(97)00105-5.

IAEA/WMO (2014). Global Network of Isotopes in Precipitation. the GNIP Database. Accessible at: http://www.iaea.org/water.

Jackson, A. S. (2009). *Variable sensitivity of European Holocene speleothems to climate change: case studies from selected caves.* Thesis.

Jex, C. N., S. J. Phipps, A. Baker, and C. Bradley (2013). Reducing uncertainty in the climatic interpretations of speleothem delta o-18. *Geophysical Research Letters 40*(10), 2259–2264.

Kottek, M., J. Grieser, C. Beck, B. Rudolf, and F. Rubel (2006). World Map of the Köppen-Geiger climate classification updated. *Meteorologische Zeitschrift 15*(3), 259–263. doi: 10.1127/0941-2948/2006/0130.

Leng, M. J. and J. D. Marshall (2004). Palaeoclimate interpretation of stable isotope data from lake sediment archives. *Quaternary Science Reviews 23*(7-8), 811–831. doi: 10.1016/j.quascirev.2003.06.012.

Li, F., X. Song, C. Tang, C. Liu, J. Yu, and W. Zhang (2007). Tracing infiltration and recharge using stable isotope in taihang mt., north china. *Environmental Geology 53*(3), 687–696.

Majoube, M. (1971). Fractionnement en oxygéne18 et en deutérium entre l'eau et sa vapeur. *Journal of Chemical Physics 197*, 1423–1436.

Mather, J. R. (1978). *The climatic water balance in environmental analysis.* Lexington, Mass., D.C. Heath and Company.

Mathieu, R. and T. Bariac (1996). An Isotopic Study (^{2}H and ^{18}O) of Water Movements in Clayey Soils Under a Semiarid Climate. *Water Resources Research 32*(4), 779–789. doi: 10.1029/96wr00074.

McCabe, G. J. and S. L. Markstrom (2007). A monthly water-balance model driven by a graphical user interface. Report, U. S. Geological Survey Open-File report 2007-1008.

McCarroll, D. and N. J. Loader (2004). Stable isotopes in tree rings. *Quaternary Science Reviews 23*(7-8), 771–801. doi: 10.1016/j.quascirev.2003.06.017.

McDermott, F. (2004). Palaeo-climate reconstruction from stable isotope variations in speleothems: a review. *Quaternary Science Reviews 23*(7-8), 901–918.

Merlivat, L. and J. Jouzel (1979). Global climatic interpretation of the deuterium-oxygen 18 relationship for precipitation. *Journal of Geophysical Research: Oceans 84*(C8), 5029–5033. doi: 10.1029/JC084iC08p05029.

Moerman, J. W., K. M. Cobb, J. W. Partin, A. N. Meckler, S. A. Carolin, J. F. Adkins, S. Lejau, J. Malang, B. Clark, and A. A. Tuen (2014). Transformation of enso-related rainwater to dripwater delta o-18 variability by vadose water mixing. *Geophysical Research Letters 41*(22), 7907–7915.

Newman, B. D., A. R. Campbell, and B. P. Wilcox (1997). Tracer-based studies of soil water movement in semi-arid forests of new mexico. *Journal of Hydrology 196*(1-4), 251–270.

Rayleigh, J. W. S. (1896). Theoretical considerations respecting the separation of gases by diffusion and similar processes. *Philosophical Magazine Series 5 42*, 493–498. doi: 10.1080/14786449608620944.

Robertson, J. A. and C. A. Gazis (2006). An oxygen isotope study of seasonal trends in soil water fluxes at two sites along a climate gradient in Washington state (USA). *Journal of Hydrology 328*(1-2), 375–387. doi: 10.1016/j.jhydrol.2005.12.031.

Rozanski, K., L. Aragus-Aragus, and R. Gonfiantini (1993). *Isotopic patterns in modern global precipitation*, pp. 1–36. Geophysical Monograph 78. Washington, DC: AGU. doi: 10.1029/GM078p0001.

Schiff, H. (1975). Berechnung der potentiellen Verdunstung und deren vergleich mit aktuellen Verdunstungswerten von Lysimetern. *Archiv für Meteorologie, Geophysik und Bioklimatologie, Serie B 23*(4), 331–342. doi: 10.1007/bf02242689.

Shurbaji, A. R. M., F. M. Phillips, A. R. Campbell, and R. G. Knowlton (1995). Application of a numerical-model for simulating water-flow, isotope transport, and heat-transfer in the unsaturated zone. *Journal of Hydrology 171*(1-2), 143–163.

Smart, P. and H. Friedrich (1986). Water movement and storage in the unsaturated zone of a maturely karstified carbonate aquifer, mendip hills, england. *Proceedings of the Environmental Problems in Karst Terranes and Their Solutions Conference. National Water Well Association, Dublin OH*, 59–87.

Tang, K. and X. Feng (2001). The effect of soil hydrology on the oxygen and hydrogen isotopic compositions of plants' source water. *Earth and Planetary Science Letters 185*(3-4), 355–367. doi: 10.1016/S0012-821X(00)00385-X.

Thornthwaite, C. W. (1948). An approach toward a rational classification of climate. *Geographical Review 38*, 55–94.

Tooth, A. F. and I. J. Fairchild (2003). Soil and karst aquifer hydrological controls on the geochemical evolution of speleothem-forming drip waters, crag cave, southwest ireland. *Journal of Hydrology 273*(1-4), 51–68.

Trajkovic, S. and S. Kolakovic (2009). Evaluation of Reference Evapotranspiration Equations Under Humid Conditions. *Water Resources Management 23*(14), 3057–3067. doi: 10.1007/s11269-009-9423-4.

Wackerbarth, A., D. Scholz, J. Fohlmeister, and A. Mangini (2010). Modelling the δ^{18}O value of cave drip water and speleothem calcite. *Earth and Planetary Science Letters 299*, 387–397. doi: 10.1016/j.epsl.2010.09.019.

Williams, P. W. (2008). The role of the epikarst in karst and cave hydrogeology: a review. *International Journal of Speleology 37*(1), 1–10.

WRB, I. W. g. (2014). World Reference Base for Soil Resources 2014. International soil classification system for naming soils and creating legends for soil maps. Report, World Soil Resources Reports No. 106. FAO, Rome.

Xu, C., M. Sano, and T. Nakatsuka (2011). Tree ring cellulose δ^{18}O of Fokienia hodginsii in northern Laos: A promising proxy to reconstruct ENSO? *Journal of Geophysical Research: Atmospheres 116*(D24), D24109. doi: 10.1029/2011jd016694.

Zimmermann, U., D. Ehhalt, and K. O. Muennich (1967). Soil water movement and evapotranspiration: changes in the isotopic composition of the water. *Proceedings of the Symposium on Isotopes in Hydrology, Int. At. Energy Agency, Vienna. 83*, 567–85.

Appendix 1. Supplementary Material

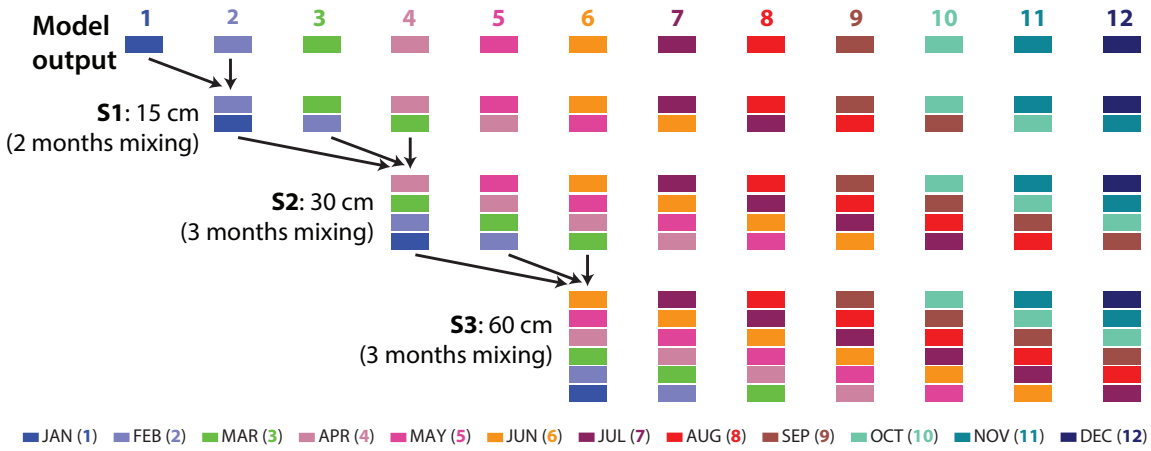

Supplementary Figure S1: *Schematic showing how the modelled $\delta^{18}O_{sw}$ is allowed to mix with antecedent water in depth. Here a sequence of 2 (S1), 3 (S2) and 3 (S3) months is illustrated. However, all combinations using 2-5 months have been calculated (see Figure 5b-d). The monthly weighting factors used to compute the mixing are based on the relative contributions of each month to the total moisture as shown in Table 1.*

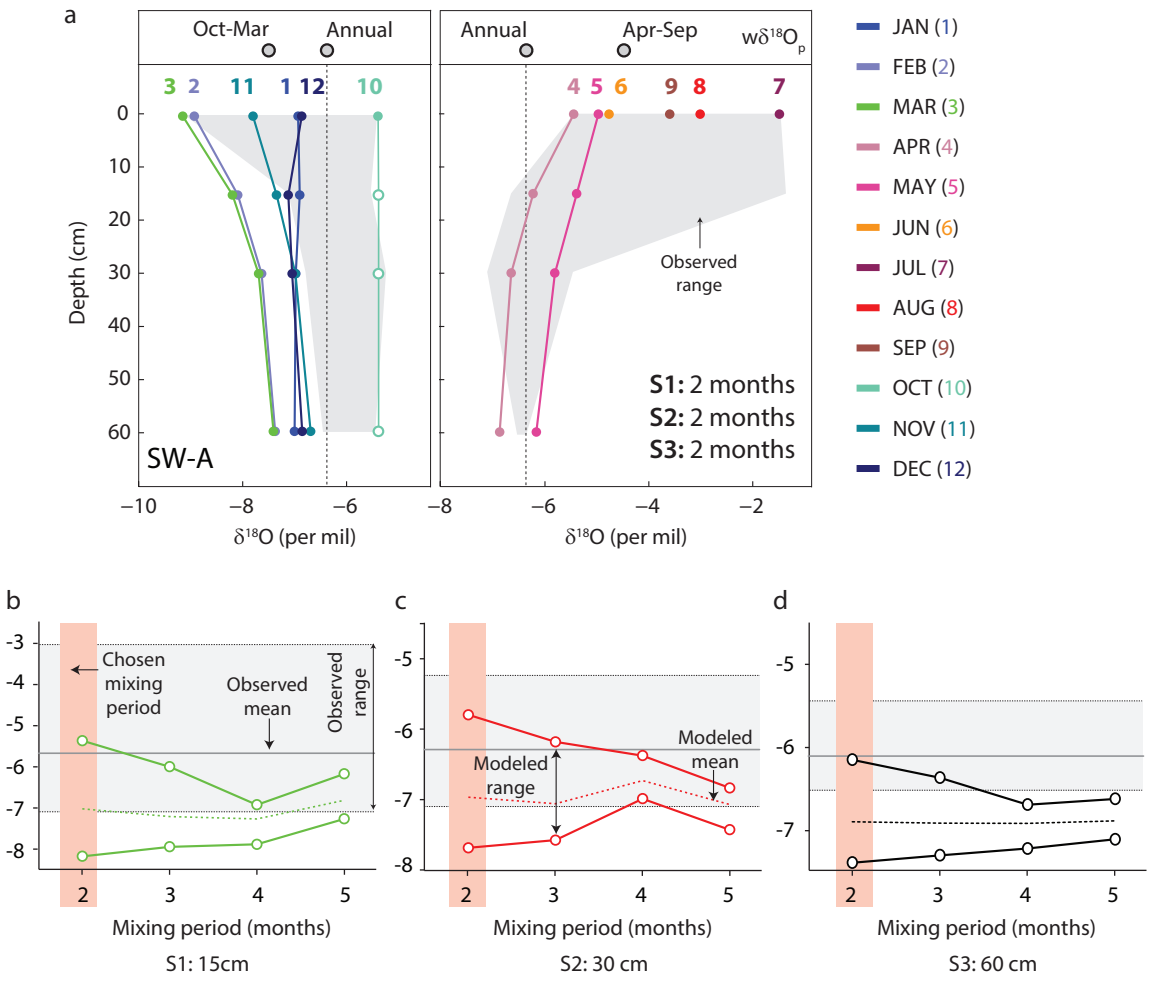

Supplementary Figure S2: *Same as Figure 5 for the soil water model considering only those months with hydrologically effective precipitation (equivalent to the approach of Wackerbarth et al., 2010). The model outputs do not agree well with observations in this case.*

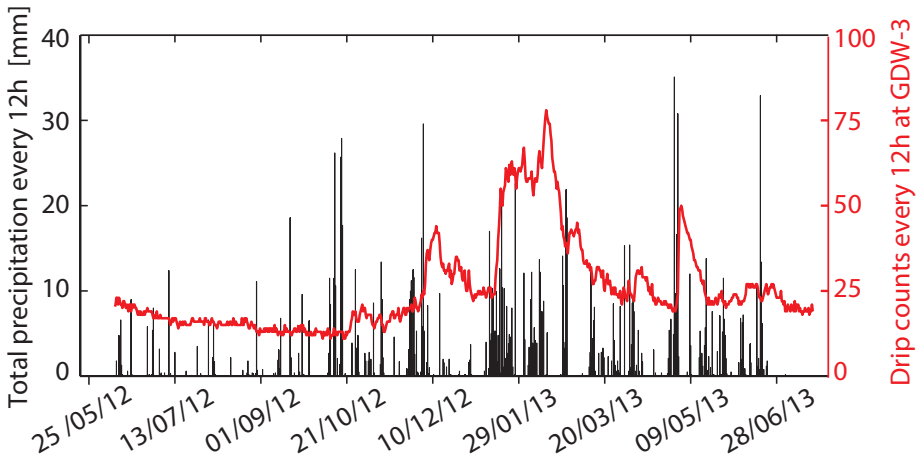

Supplementary Figure S3: *Total precipitation at Santander Airport meteorological station (AEMET; left y-axis) and drip counts every 12h the GDW-3 drip site (right y-axis) for the period between June 2012 and July 2013. Drip counts were measured with a self-contained automated drip counter device (Stalagmate Plus Mk2b). See Figure 1 for the exact location of the GDW-3 drip site in the cave gallery.*

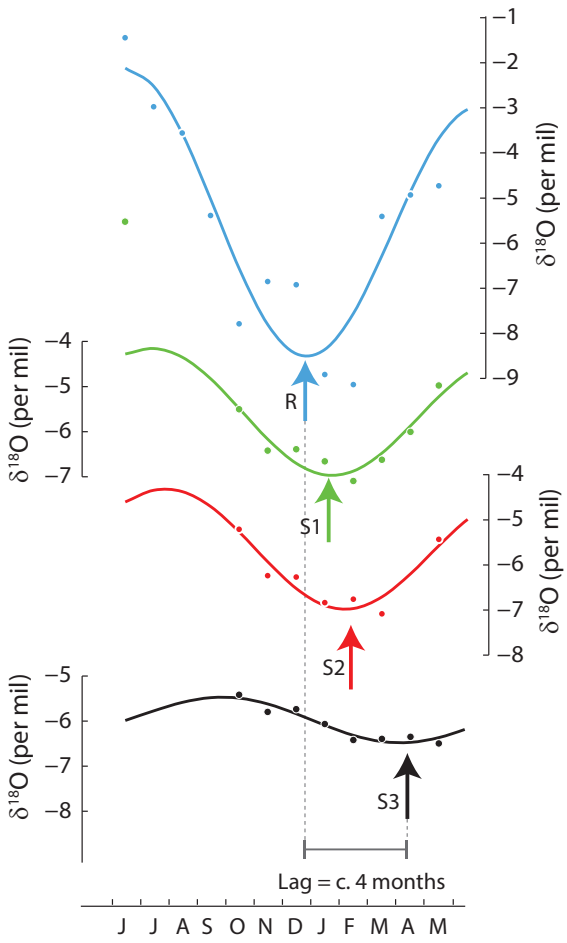

Supplementary Figure S4: *Sinusoidal curves have been fitted to the measured $\delta^{18}O_p$ (blue curve) and $\delta^{18}O_{sw}$ data for 15 cm, 30 cm and 60 cm (green, red and black curves respectively) to illustrate the nature of the lags and attenuation of the seasonal $\delta^{18}O_{sw}$ signal in the soil-waters.*

Sample ID	Type	Install date	Collection date	δD	St.d	$\delta^{18}O$	St.d
GAR-R1	Rain	30/06/2012	30/07/2012	-5.6	0.32	-1.49	0.13
GAR -R2	Rain	30/07/2012	30/08/2012	-11.42	0.63	-3.01	0.08
GAR -R13	Rain	30/08/2012	01/10/2012	-12.83	0.02	-3.59	0.01
GAR -R3	Rain	01/10/2012	30/10/2012	-25.64	0.15	-5.42	0.04
GAR -R4	Rain	30/10/2012	30/11/2012	-40.34	0.1	-7.81	0.01
GAR -R5	Rain	30/11/2012	30/12/2012	-35.35	0.14	-6.88	0.02
GAR -R6	Rain	30/12/2012	24/01/2013	-35.1	0.11	-6.95	0.02
GAR -R8	Rain	24/01/2013	01/03/2013	-48.87	0.04	-8.93	0.01
GAR -R9	Rain	01/03/2013	27/03/2013	-57.69	0.12	-9.15	0.05
GAR -R10	Rain	27/03/2013	30/04/2013	-24.31	0.19	-5.44	0.03
GAR -R11	Rain	30/04/2013	30/05/2013	-22.48	0.06	-4.97	0.02
GAR -R12	Rain	30/05/2013	18/06/2013	-26.56	0.21	-4.76	0.01
GAR -S1.1	15 cm	30/06/2012	30/07/2012	-4.44	0.36	-1.39	0.04
GAR -S1.2	15 cm	30/07/2012	30/08/2012	-	-	-	-
GAR -S1.13	15 cm	30/08/2012	01/10/2012	-	-	-	-
GAR -S1.3	15 cm	01/10/2012	30/10/2012	-	-	-	-
GAR -S1.4	15 cm	30/10/2012	30/11/2012	-26.59	0.06	-5.54	0.02
GAR -S1.5	15 cm	30/11/2012	30/12/2012	-32.48	0.46	-6.45	0.07
GAR -S1.7	15 cm	30/12/2012	30/01/2013	-32.9	0.2	-6.42	0.06
GAR -S1.8	15 cm	30/01/2013	01/03/2013	-34.73	0.3	-6.69	0.06
GAR -S1.9	15 cm	01/03/2013	27/03/2013	-36.58	0.46	-7.12	0.04
GAR -S1.10	15 cm	27/03/2013	30/04/2013	-34.83	0.18	-6.65	0.02
GAR -S1.11	15 cm	30/04/2013	30/05/2013	-31.26	0.06	-6.03	0.04
GAR -S1.12	15 cm	30/05/2013	18/06/2013	-24.42	0.24	-5.01	0.06
GAR -S2.1	30 cm	30/06/2012	30/07/2012	-	-	-	-
GAR -S2.2	30 cm	30/07/2012	30/08/2012	-	-	-	-
GAR -S2.13	30 cm	30/08/2012	01/10/2012	-	-	-	-
GAR -S2.3	30 cm	01/10/2012	30/10/2012	-	-	-	-
GAR -S2.4	30 cm	30/10/2012	30/11/2012	-24.11	0.48	-5.24	0.01
GAR -S2.5	30 cm	30/11/2012	30/12/2012	-30.06	0.43	-6.26	0.07
GAR -S2.6	30 cm	30/12/2012	24/01/2013	-30.33	0.41	-6.3	0.05
GAR -S2.8	30 cm	24/01/2013	01/03/2013	-37.24	0.11	-6.86	0.04
GAR -S2.9	30 cm	01/03/2013	27/03/2013	-33.75	0.32	-6.79	0
GAR -S2.10	30 cm	27/03/2013	30/04/2013	-38.04	0.03	-7.11	0.06
GAR -S2.11	30 cm	30/04/2013	30/05/2013	-	-	-	-
GAR -S2.12	30 cm	30/05/2013	18/06/2013	-29.14	0.13	-5.46	0
GAR -S3.1	60 cm	30/06/2012	30/07/2012	-	-	-	-
GAR -S3.2	60 cm	30/07/2012	30/08/2012	-	-	-	-
GAR -S3.13	60 cm	30/08/2012	01/10/2012	-	-	-	-
GAR -S3.3	60 cm	01/10/2012	30/10/2012	-	-	-	-
GAR -S3.4	60 cm	30/10/2012	30/11/2012	-27.14	0	-5.45	0
GAR -S3.5	60 cm	30/11/2012	30/12/2012	-28.15	0.19	-5.82	0.1
GAR -S3.6	60 cm	30/12/2012	24/01/2013	-28.1	0.5	-5.76	0.03
GAR -S3.8	60 cm	24/01/2013	01/03/2013	-30.14	0.24	-6.1	0.01
GAR -S3.9	60 cm	01/03/2013	27/03/2013	-33.19	0.33	-6.45	0.01
GAR -S3.10	60 cm	27/03/2013	30/04/2013	-33.02	0.11	-6.42	0.04
GAR -S3.11	60 cm	30/04/2013	30/05/2013	-33.6	0.2	-6.38	0.06
GAR -S3.12	60 cm	30/05/2013	18/06/2013	-34.28	0.63	-6.52	0.1

Supplementary Table S1: *Details of the $\delta^{18}O$ and δD measurements of all samples. St.d are measurement standard deviations.*